*Progress In Electromagnetics Research, PIER 83, 353–374, 2008*

# ELECTROMAGNETIC MODELING OF RETINAL PHOTORECEPTORS

**C. Canbay and İ. Ünal**

Department of Electrical and Electronics Engineering
Yeditepe University
26 Ağustos Yerleşimi, Kayışdağı, 34755, İstanbul, Turkey

**Abstract**—New electromagnetic models for the rods and cones that are the photoreceptors at the back of the retina are developed and simulated in order to explain the roles of dimension, geometrical structure, directional sensitivity and visual pigments of the photoreceptors in the reception of visible light. The rods and cones are modeled as uniform and quasi-tapered helical antennas, respectively. The results of the model study show that if the model antennas have the original photoreceptor cell dimensions, the frequency responses of the model antennas and the spectral sensitivities of the photoreceptors would be very close to each other. In addition, it's observed that the spectral sensitivities of $L$, $M$ and $S$ cones are broadband over the visible light spectrum, and there are secondary peaks beside main peaks in the spectral sensitivity curves of the cones, because of the conical shape of the cones. It's also observed that there is only one main peak in the spectral sensitivity curves of the rods, because of the uniform and cylindrical shape of the rods. Finally, an array of the novel modeled antennas is also discussed to be used in biomedical applications of artificial retinal photoreceptors in medicine, although the main scope is not designing artificial retinal photoreceptor prosthesis.

## 1. INTRODUCTION

Eyes are amazing sensory organs that allow us to percept all the beauty of the world we live in, to read and gain knowledge, and to communicate to each other through visual expression and visual arts. The eye is a principal optical device designed to focus the visual images on the retina. Journey of the light, which has a dual nature as wave and particle, starts with the cornea and lens. Next, it traverses the vitreous humour which fills the eye cavity before being absorbed by the

photoreceptor cells that are the rods and cones. The incoming light waves are converted to the electrical signals that stimulate neurons in the retina [1, 2].

Although this general visual mechanism seems to be well discovered and explained, neurobiologists still research on the details of the circuit that subserves trichromatic color vision in human eyes [3]. Human trichromatic color vision depends on three types of the cones with different spectral sensitivities. However, some of the fundamental questions about the human color vision have remained under research, until today: (a) What is the reason of geometrical shape differences between the cones and rods? (b) Is the spectral sensitivity attributable to only visual pigments, but also the dimension and geometrical shape of the photoreceptors? Beside these, discussions about the theory of different spectral absorptions of three pigments and three cones have been given in the literature [1, 4, 5].

The trichromatic theory was first proposed by Young [6] and was further explored by Helmholtz in 1866. This theory is primarily based on color mixing experiment and suggests that a combination of three channels explain color discrimination functions. Present-day theories of color vision state that there are only three pigments in the outer segments of the cones of human eye, and spectral sensitivities of the three cones differ because of genetic differences of their visual pigments, and the underlying mechanisms have been well explored and proved by many visual scientists [7–12].

Although there are experimental evidences of genetic differences between each visual pigment, the effects of size, shape [13, 14] and physical structure of the cones shouldn't be neglected for the spectral discrimination mechanism. Sheppard [1] suggests that the spectral selectivity of an individual cone might be substantially affected by its physical characteristics (size, index of refraction, etc.) as well as by any photopigment that it might contain. Radiant energy can be propagated in human cone outer segments with waveguide modal patterns. Coupled with a variation in outer segment diameters and indices of refraction, such a modal propagation could provide the cones with a spectral discrimination mechanism. Miller [15] comments that, the size of the important elements of the cornea, eye lens, and retina are of the order of the wavelengths of visible light or a fraction thereof, and can therefore make these organs transparent to visible light. The size of a foveal cone is thus very much tuned to the wavelength of visible light. The unique essence of the vertebrate eye is that the structure of the transparent optical components, the rhodopsin molecule, and the size of the foveal cones are all tuned to interact optimally with wavelengths of visible light. The receiving of light waves by both the

rods and cones is not only governed by the specific chemical nature of the opsin-chromophore relationship, but also by the physical structure of the photoreceptor cells [16]. The optical sensitivity of an eye depends on its photoreceptor length and diameter, as well as pupil diameter and focal length of the eye, and also wavelength of operation [17]. Kraus and Marhefka [18] explain the electromagnetic radiation mechanism of the rods and cones, along their axes. The existence of waveguide modal patterns in human cone outer segments and the optical properties of the retinal photoreceptors had been demonstrated by Enoch [19, 20] and Pask and Stacey [21]. Results of a more recent work on the analysis of the light propagation in the human photoreceptor cells using numerical electromagnetic (FDTD) methods [22] also suggests that the variation in cone shape and size plays a role in color discrimination of human visual system.

The uniform and quasi-tapered helical antennas are simplified representations of the rod outer segments (ROS) and cone outer segments (COS), respectively. Thus, the rods and cones can be modeled as the uniform and quasi-tapered helical antennas, respectively, that have physical dimensions on the same order of the human rod and cone photoreceptors. These models will lead to understand the effects of photoreceptors' dimension, geometrical structure and visual pigments on spectral discrimination mechanism. It is obvious that the photoreceptors are not completely like wire antennas and the electrical parameters of the photoreceptor cells are different from conductors. However, if an electromagnetic wave comes onto a medium whose dispersive dielectric permittivity $\varepsilon$ is different than $\varepsilon_0$, even conductivity $\sigma$ is equal to zero, a current distribution can be induced on the medium. The total current density consists of the conduction current density $\mathbf{J}_c$ and equivalent current density $\mathbf{J}_{eq}$ on biological tissues can be defined as

$$\mathbf{J}_c = \sigma\,\mathbf{E} \tag{1}$$

$$\mathbf{J}_{eq} = j\,\omega\,(\varepsilon - \varepsilon_0)\,\mathbf{E} \tag{2}$$

In this study, the effects of the size and shape of the photoreceptors in the reception of visible light are explained from a different way by developing models which give convenient and close results for the spectral sensitivity curves of the photoreceptors. Naturally, the biological tissues such as the photoreceptors cannot operate as efficient as conducting wire antennas, too.

New theoretical photoreceptor models are proposed for the human retina by using the analytic and modeling techniques in electromagnetic theory to explain the receiving mechanism of the photoreceptor cells and also the roles of dimension,

geometrical structure, directional sensitivity and visual pigments of the photoreceptors in the reception of visible light. The rod cells receiving the color of the center wavelength of 498 nm are modeled as the uniform helical antennas. The frequency responses of the modeled uniform helical antennas for the rods are explained, and the results are compared with the frequency responses of the original rod cells [1, 23]. The radiation (or reception) diagrams of the modeled uniform helical antennas are calculated and simulated.

In addition, before modeling of the cones, the gain-wavelength response of a conical helical antenna is compared with the spectral sensitivity curves of the cone cells, and the similarities are explained. The analyses show that the fundamental colors such as red, green and blue can be received by each type of the cones with different intensities, making maxima at different wavelengths. It's also explained and discussed that the spectral sensitivities of $L$, $M$ and $S$ cones are broadband over the visible light spectrum, because of their conical and tapered shapes. On the other hand the rod cells have narrower bandwidth, because of their cylindrical and uniform shapes.

An antenna array of the quasi-tapered helical antennas is used to model the cone cells that are connected to each other by diffuse cone bipolar cells. The results of the frequency responses of the modeled quasi-tapered helical antennas are compared with the frequency responses of the original cone cells [24, 25]. The radiation (or reception) diagrams of the modeled quasi-tapered helical antennas are calculated and simulated. The modeling study of the quasi-tapered helical antenna array verifies the enhancement structure of the photoreceptor array for the visual resolution and the directional sensitivity feature of the photoreceptors. Although the main intention is not designing an artificial retinal photoreceptor prosthesis, the modeled array is also suggested and discussed to be used in biomedical applications of the artificial photoreceptors of a retinal visual prosthesis, in the future. The contributions of the inverse alignment of the photoreceptors with respect to the incoming light, in the reception of visible light is also explained and supported with the theoretical results.

## 2. METHODS

The geometrical parameters of a helical antenna are the turn number $N$, the diameter of one coil $D$, the spacing between each turn $S$, the wire length of one coil $L_o$, the antenna length $L_n$, the pitch angle $\alpha$ and the circumference $C$ as shown in Fig. 1(a).

A helical antenna can operate in many modes; however, normal (broadside) and axial modes are the major ones. Lee et al. [26]

proposed the theory on the frequency responses of the uniform helical antennas and quasi-tapered helical antennas consisting of two uniform sections.

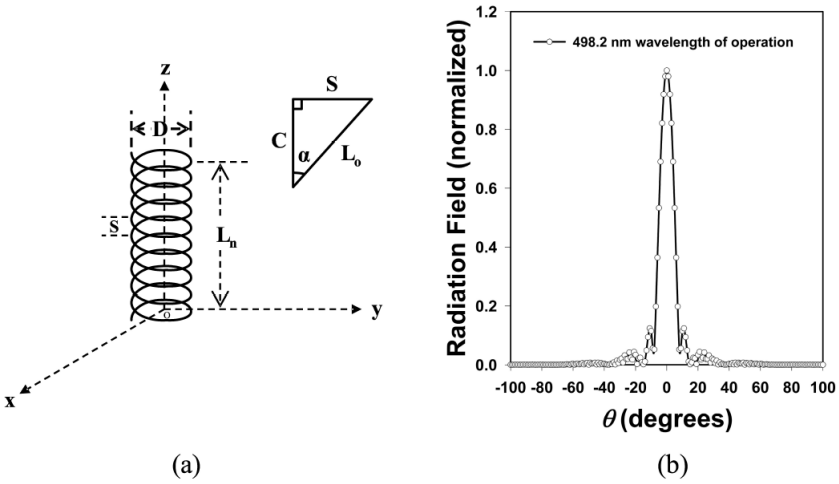


(a) (b)

**Figure 1.** Illustration of (a) the geometrical parameters of the uniform helical antenna and (b) the radiation (or reception) pattern ($E$-plane) of the simulated uniform helical antenna for the rod cell.

Since the index of refraction of the tissue (cladding) which surrounds the photoreceptor cells is approximately equal to the value of the vitreous humour (around 1.336 at visible light frequencies) [27, 28] and also depends on frequency [29], the computations of electromagnetic fields of the modeled uniform and quasi-tapered helical antennas are realized in the dispersive vitreous humour. The modeled uniform and quasi-tapered helical antennas are assumed to operate in the isotropic dispersive medium which is different from free space. The far-zone electric field intensity of a uniform helical antenna located in the dispersive media can be found as

$$\mathbf{E} = \frac{-j\,\gamma\,\omega}{\eta}\,\frac{1}{(\sigma + j\,\omega\,\varepsilon_0\,\varepsilon_r)}\,\mathbf{A} \tag{3}$$

where $\mathbf{A}$ is the retarded magnetic vector potential, $\eta$ is the characteristic impedance and $\gamma$ is the propagation constant of the medium [30], $\sigma$ is the conductivity of the medium at low frequencies, $\omega$ is the angular frequency, $\varepsilon_0$ is the absolute dielectric permittivity of free space and $\varepsilon_r$ is the relative dielectric permittivity of the medium which is dispersive and can be expanded as $\varepsilon_r = \varepsilon_r' - j\varepsilon_r''$ [28, 29, 31, 32], where

$\varepsilon_r'$ is the real part of the relative dielectric permittivity of the medium and $\varepsilon_r''$ is the imaginary part of the relative dielectric permittivity of the medium. The retarded magnetic vector potential of a uniform helical antenna is defined as

$$\begin{aligned}\mathbf{A} \;=\; & \frac{\mu_0\, a\, \exp(-\gamma\, r)}{4\,\pi\, r} \\ & \times \left\{ \int_0^{\varphi_m'} \exp(-j\, d\, \varphi')\, [-\hat{\mathbf{x}}\, \sin\varphi' \;+\; \hat{\mathbf{y}}\, \cos\varphi' \;+\; \hat{\mathbf{z}}\, \tan\alpha] \right. \\ & \times \left[ J_0(u) + 2\sum_{b=1}^{\infty}(-1)^b\, \cos[2b\,(\varphi-\varphi')]\, J_{2b}(u) \right. \\ & \left. \left. +2j\sum_{b=0}^{\infty}(-1)^b\, \cos[(2b+1)\,(\varphi-\varphi')]\, J_{2b+1}(u) \right] d\varphi' \right\} \end{aligned} \tag{4}$$

where $a$ is the radius of the helix, $r$ is the radial distance of the observation point, $\varphi_m'$, $u$ and $d$ are given by Lee et al. [26], $\mu_0$ is the permeability of free space, $\varphi$ is the angle between $x$-axis and the projection of position vector on $(x-y)$ plane, $J_I$ is the Bessel function of the first kind of order $I$, $J_0$ is the Bessel function of the first kind of order zero, $J_{2b}$ and $J_{2b+1}$ are the Bessel functions of the first kind of order $2b$ and $2b+1$, respectively.

There are some theoretical [18, 26], empirical [33] and numerical approaches [34] for the gain responses of the helical antennas. Due to the theoretical difficulties, there is no study in the literature for calculating the gain of helical antennas that are modeled in the real rod and cone dimensions with the turn diameter of 1–2 μm, the turn number of more than 100 and the small pitch angle of 0.3°–0.5°. Therefore, the gain responses of the modeled antennas are found by using the duality principle and modeling techniques in electromagnetic theory, and empirical equations [33]. The gain response calculation [33] based on the empirical peak value of the gain expression for the antenna modeling is determined by

$$G_p = 8.3 \left(\frac{\pi\, D}{\lambda_p}\right)^{\sqrt{N+2}-1} \left(\frac{N\, S}{\lambda_p}\right)^{0.8} \left(\frac{\tan 12.5^\circ}{\tan\alpha}\right)^{\sqrt{N}/2} \tag{5}$$

where $\lambda_p$ is the wavelength at the peak value of the gain.

## 3. RESULTS

### 3.1. Modeling of the Rod Cells as the Uniform Helical Antennas

In most cases, it is either difficult or impractical to find the radiation patterns and impedances of actual antennas. In this situation, a scale model of the antenna system can be built in order to transform into a suitable size. Then, the computations and measurements may be performed to study the model's properties under various conditions. A length $L_{act}$ on an actual antenna is proportionally related to the corresponding dimension $L_{mod}$ on the model antenna by a scale factor $k_r$. The wavelength $\lambda_{mod}$ used with the model antenna and the wavelength $\lambda_{act}$ used with the actual antenna are inversely proportional by the same scale factor [35].

According to the experimental results, the pitch angle and turn numbers do not affect the frequency at the peak value of the gain of the helical antenna [33]. Firstly, the experimental peak value of the gain result of the helical antenna designed at approximately 1 GHz frequency and operating in free space [33] is considered for the modeling. This uniform helical antenna has the geometrical parameters of the turn number of 10, the pitch angle of 12.5° and the turn diameter of 0.1075 m. Using Eq. (5) and the experimental gain result of this helical antenna, the wavelength at the peak value of gain of the antenna with the turn number of about 800, the pitch angle of about 0.3°–0.4°, the turn diameter of 0.1075 m, is calculated as about 0.037177 m in the vitreous humour. Since the modeled uniform helical antenna operating in the vitreous humour would have a peak gain at around 498 nm wavelength, then the scale factor is obtained as $7.465 \times 10^4$.

The diameters of the rod outer segment (ROS) and cone outer segment (COS) vary between 1–3 microns [1, 13, 15, 27, 28]. The spacing between each fold is between 24–30 nm [36, 37]. The outer segment length varies between 6–50 microns and the fold number varies between 200–1600 turns [27, 36, 37].

Taking into account the scale factor and assuming that the helical antenna parameters have the original rod cell dimensions, the geometrical parameters of the uniform helical antenna are calculated as 1.44 μm diameter, 0.365° pitch angle, 800 turn number, 28.82 nm spacing and 23.06 μm antenna length. The radiation (or reception) pattern of the modeled uniform helical antenna with respect to $\theta$, which is the angle between the antenna placement ($z$-axis) and the position vector, is simulated by using Kai-Fong Lee's approach [26] (Fig. 1(b)).

### 3.2. Effects of the Geometrical Shapes of the Photoreceptors on Their Spectral Sensitivities

The figures, which have been taken by means of the electron microscope [13, 14], show that the geometrical structures of the rods and cones are similarly in the shapes of the cylindrical helical antennas and quasi-tapered helical antennas, respectively. The logarithmic spectral sensitivity curves of the cones are given in Fig. 2(a) [24]. Sheppard [1] had noted the secondary maxima beside the main peaks of the curves of the spectral sensitivities of the cones. The gain-wavelength response of a conical helical antenna is studied experimentally by Wong and King [38], as in Fig. 2(b). The conical and quasi-tapered helix type antennas exhibit broad bandwidth characteristics with respect to the radiation pattern and the input impedance [38–41]. Moreover, tapered and conical structures designed as antennas generally have well known broadband characteristics [42–47]. The wavelength response curves of both the conical helical antenna and the cones show approximately same characteristics with one main peak and one secondary peak over the wavelength. In addition, if the frequency responses of uniform helical antennas [38] are compared with the spectral sensitivity curves of the rods [1, 23], it can be seen that there is only one main peak in their frequency responses. This analysis is able to explain the reasons of the conical and tapered helix shapes

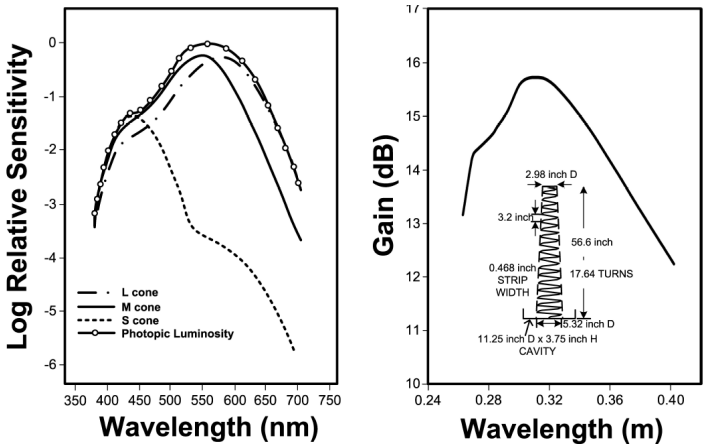


**Figure 2.** Schematic representations of (a) the spectral sensitivities of the cone cells (Reproduced [24], p.1292), (b) the gain-wavelength response of a conical helical antenna (Reproduced [38], p.76).

of the cones, and also the cylindrical helix shapes of the rods. Because of the uniform and cylindrical shape of the rods, there is only one main peak in the spectral sensitivity curves of the rods. Because of the conical shape of the cones, there are secondary peaks beside main peaks in the broadband spectral sensitivity curves of the cones.

Taper of the helical antennas also acts as a transformer to match the antenna and the free space, with decreased reflections in the current distribution [48]. Tapering mechanism of the cones acts to make the transfer of energy more efficient, just like an impedance-matching device, too [20]. Although there is no one to one relationship, the solar cells currently have antireflective pyramidal-textured coating rather than a flat one for the reduction of the optical losses [49]. Another analogy is pyramidal or conical absorber materials used in anechoic chamber laboratories. Hence, a cone cell can (efficiently) receive the three bands of the visible color at different intensities, making maxima at different wavelengths, because of its conical and tapered geometrical shape.

### 3.3. Importance of Dimensions and Visual Pigments of the Photoreceptors on Their Spectral Sensitivities

The cone dimensions vary greatly in form; those in the fovea are slender, like the rods, although their morphology and staining characteristics are always those of cones. However, in the periphery they become short and thick. The average numerical dimension values for the cones in the different regions of the retina are given in literature [27].

Little changes in uniform and non-uniform helical antenna dimensions (especially diameters) lead different frequency responses in the computations and experiments (Fig. 3) [33, 38]. The irregular geometrical structures of the photoreceptors are not absolutely the same as each other, even in the same region of the retina. Hence, it's expected that the spectral responses of each photoreceptor cell with different shapes can be different from each other, by minor discriminations.

Visual pigments are placed in the photoreceptor tissue whose electrical properties can be expressed as tensor [16, 50]. The absorption of the visual pigments depends on the relative position and orientation of electromagnetic fields. Spatial arrangement of the pigments inside the photoreceptors is also effective in the spectral properties of the photoreceptors [50]. In fact, the propagation ways of light waves in human eye are frequency-dispersive lossy dielectric media, including the photoreceptors itself. Therefore, since the absorbed energy level is proportional to complex dispersive conductivity of the medium,

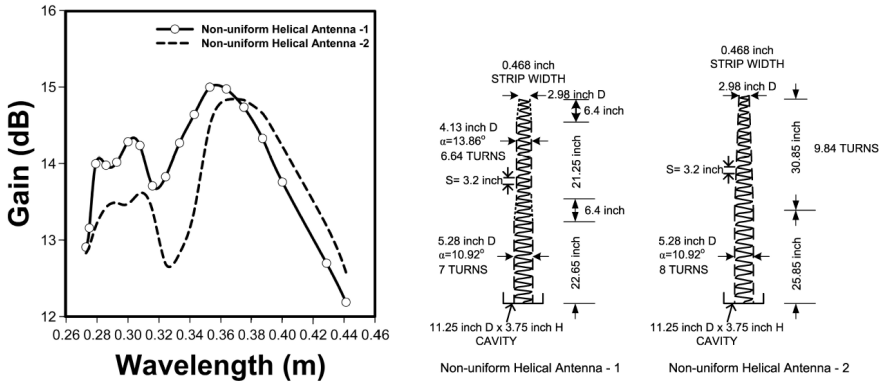


**Figure 3.** Schematic representations of the gain-wavelength responses of two non-uniform helical antennas (Reproduced [38], p.77).

the visual pigments characterize the quality of the efficiency of the photoreceptors beside their effects on spectral sensitivity. Enoch and Fry [51] had analyzed the characteristics of a retinal photoreceptor by modeling as a cone supported horn antenna with and without polystyrene-foam, at microwave frequencies. The cone supported horn antenna with polystyrene-foam absorbed more power than the one without polystyrene-foam [51]. Visual pigments are efficient materials absorbing electromagnetic waves at specific frequencies, from antenna engineering point of view. If an antenna wire is made of different materials which can be considered as visual pigments within the photoreceptor tissue, obviously the gain responses would be different from each other. Hence, visual pigments would have importance on both efficiency and spectral sensitivity.

The antenna models could also be analyzed from atomic scale point of view, such as electron mobility, drift motion and free electrons, inside the wire of the antennas. In spite of the existence of the physical and chemical reactions of the visual pigments inside the photoreceptors, the visual pigments are related to the material specifications of antenna wire, from a macroscopic scale point of view. When a modulated sine wave enters a frequency-dispersive lossy dielectric medium, the wave shows the behavior of the pulse distortion with decreased intensity [52–54]. After the light waves excite the vitreous humour and photoreceptors, the optical information is modulated and converted to electrical signals, matching the Hodgkin-Huxley model of the action potential [55]. The photoreceptors behave as both antennas and partially frequency converters, from antenna engineering point of view.

### 3.4. Modeling of the Array Structure of the Cones

An array of model antennas for the cone cells is developed to analyze the resonance characteristics of the cone cells at visible light frequencies and also to investigate the photoreceptor array structure for enhancement of the visual resolution. Beside, the array of model antennas can also be used in biomedical applications of the artificial retinal photoreceptors in medicine, for the future applications. For analyzing and simulating to see how such an array model would work, a quasi-tapered helical antenna with twenty-one sections receiving all colors covering red, green and blue is used for modeling of the cones, as an array element. $L$ and $M$ cones are randomly arranged in the central fovea [56] and the cones are present in variable proportions, in different individuals [57, 58]. In fact, it would be very difficult to replace separate antenna models of $L$, $M$ and $S$ cones according to their appropriate spatial arrangements in the retina during medical operations. Hence, although the cones do not receive all colors at the same intensity level, such an array element can be very convenient for especially practical purposes.

The number of the uniform sections for the quasi-tapered helical antennas can be taken as infinite. The analyses of radiation diagrams (at different wavelengths of operation) of quasi-tapered helical antennas with the same frequency responses and the same lengths showed that the radiation diagrams (especially half-power beamwidth and side lobe characteristics) do not change so much after roughly 21 sections. Hence, for simplicity in the computations, a quasi-tapered helical antenna is considered for modeling to consist of twenty-one uniform sections ($\xi = 1, 2, 3, \ldots, 21$) with diameters $D_1, D_2, D_3, \ldots, D_{21}$ joined by short quasi-tapered transitions as shown in Fig. 4(a). Since the quasi-tapered helical antennas will operate in the vitreous humour medium, the far-zone electric field can be calculated as a superposition of the fields due to the twenty-one uniform sections by regarding the phase differences relative to the previous sections [26, 59].

Applying the same modeling techniques (in Sec. 3.1) for the cone cell and using Eq. (5), the operation wavelengths at the peak value of the gain of the first, second, third, ..., twenty-first sections are found as 559.10 nm, 552.99 nm, 546.88 nm, 540.77 nm, 534.66 nm, 528.55 nm, 522.44 nm, 516.33 nm, 510.22 nm, 504.11 nm, 498.00 nm, 491.89 nm, 485.78 nm, 479.67 nm, 473.56 nm, 467.45 nm, 461.34 nm, 455.23 nm, 449.12 nm, 443.01 nm and 436.90 nm, respectively. The parameters of the quasi-tapered helical antenna sections are considered to be the original cone cell dimensions. Taking into account the scale factors for each wavelength, the calculated geometrical parameters of all twenty-

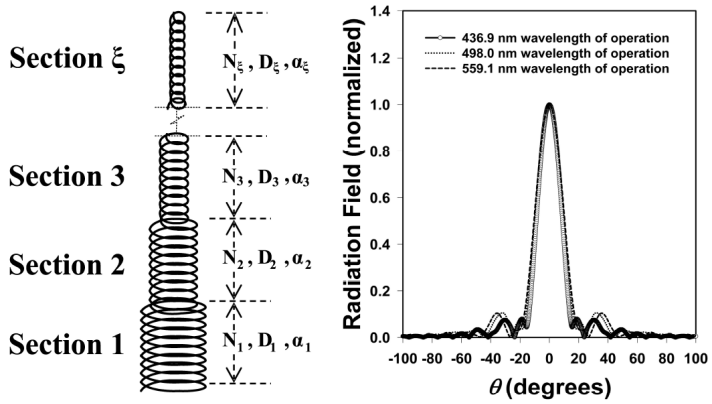


**Figure 4.** Illustration of (a) the geometrical parameters of the quasi-tapered helical antenna and (b) the radiation (or reception) pattern ($E$-plane) of the simulated quasi-tapered helical antenna for the cone cells.

one sections of the quasi-tapered helical antenna are $D_1 = 1.500\,\mu m$, $D_2 = 1.473\,\mu m$, $D_3 = 1.446\,\mu m$, $D_4 = 1.419\,\mu m$, $D_5 = 1.392\,\mu m$, $D_6 = 1.365\,\mu m$, $D_7 = 1.338\,\mu m$, $D_8 = 1.311\,\mu m$, $D_9 = 1.284\,\mu m$, $D_{10} = 1.257\,\mu m$, $D_{11} = 1.230\,\mu m$, $D_{12} = 1.203\,\mu m$, $D_{13} = 1.176\,\mu m$, $D_{14} = 1.149\,\mu m$, $D_{15} = 1.122\,\mu m$, $D_{16} = 1.095\,\mu m$, $D_{17} = 1.068\,\mu m$, $D_{18} = 1.041\,\mu m$, $D_{19} = 1.014\,\mu m$, $D_{20} = 0.987\,\mu m$, $D_{21} = 0.960\,\mu m$, diameter; $\alpha_1 = 0.3183°$, $\alpha_2 = 0.3230°$, $\alpha_3 = 0.3280°$, $\alpha_4 = 0.3334°$, $\alpha_5 = 0.3390°$, $\alpha_6 = 0.3448°$, $\alpha_7 = 0.3509°$, $\alpha_8 = 0.3574°$, $\alpha_9 = 0.3643°$, $\alpha_{10} = 0.3715°$, $\alpha_{11} = 0.3790°$, $\alpha_{12} = 0.3871°$, $\alpha_{13} = 0.3955°$, $\alpha_{14} = 0.4046°$, $\alpha_{15} = 0.4135°$, $\alpha_{16} = 0.4248°$, $\alpha_{17} = 0.4357°$, $\alpha_{18} = 0.4473°$, $\alpha_{19} = 0.4598°$, $\alpha_{20} = 0.4682°$, $\alpha_{21} = 0.4975°$ pitch angle; $N_1 = 98.4$, $N_2 = 98.8$, $N_3 = 99.1$, $N_4 = 99.3$, $N_5 = 99.6$, $N_6 = 99.8$, $N_7 = 100.1$, $N_8 = 100.3$, $N_9 = 100.4$, $N_{10} = 100.6$, $N_{11} = 100.8$, $N_{12} = 100.9$, $N_{13} = 101.0$, $N_{14} = 101.1$, $N_{15} = 101.3$, $N_{16} = 101.0$, $N_{17} = 103.6$, $N_{18} = 100.9$, $N_{19} = 100.8$, $N_{20} = 100.7$, $N_{21} = 98.4$ turn number; 25.68 nm average spacing; and 54.1 μm total antenna length. Using the empirical bandwidth frequency ratio equation [33], the ratio of the high cut-off wavelength to low cut-off wavelength is calculated for all sections approximately as ∼1.107. The bandwidth of the modeled quasi-tapered helical antenna covers the frequency responses of the colors such as red, green and blue [23–25].

The radiation (or reception) pattern of the simulated quasi-tapered helical antenna is calculated by using Eq. (3) and regarding the phase differences between the first, second, third, ..., twenty-first

sections of the antenna (Fig. 4(b)).

Two different types of cone bipolar cells are present in human retina. They are known as diffuse cone and midget bipolar cells. The midget bipolar cells are concerned only with single cone contacts in a one to one relationship. Some of the diffuse cone bipolar cells are very wide field in dendritic spread and connect with as many as 15–20 cones [60]. Commonly the smaller diffuse bipolar cells collect information from 5–7 cones in central retina, 12–14 cones in peripheral retina (Fig. 5).

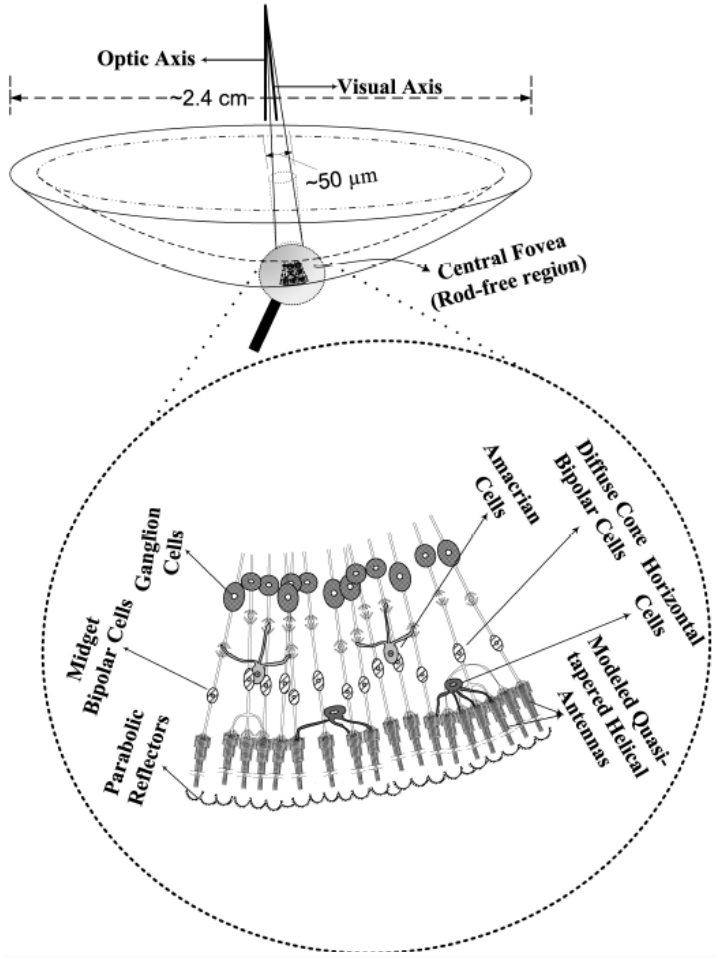


**Figure 5.** Schematic representation of the central fovea (rod-free region) of the retina and the modeled quasi-tapered helical antennas.

A simple $4 \times 4$ planar antenna array can be used to model 16 cone cells which are connected to each other by diffuse cone bipolar cells. The cones are replaced by the modeled quasi-tapered helical antennas, and considered as an array by using array theory with array factor calculation [59]. The distances and the phase differences between each cone are taken as about 0.58 μm [61] and 0°, respectively; and also the wavelength of operation is taken as 559.1 nm, arbitrarily. The computed and simulated radiation (or reception) patterns of the modeled quasi-tapered helical antenna and the array of the modeled quasi-tapered helical antennas, respectively, disregarding the mutual coupling effects, are given in Fig. 6. The half-power beamwidth of the radiation (or reception) pattern of the modeled antenna array as well as the side lobe levels have decreased. When different wavelengths of operation are applied, instead of 559.1 nm, the half-power beamwidth and the side lobes change insignificantly. Consequently, it is verified that the photoreceptor cells are arranged as an array to improve the spatial resolution by reducing noise level [62].

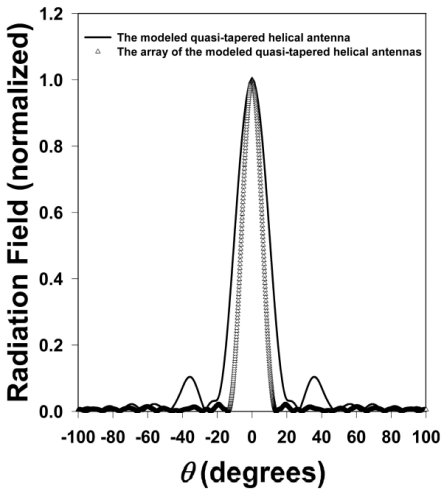


**Figure 6.** Illustration of the radiation (or reception) patterns ($E$-plane) of the simulated quasi-tapered helical antenna element, and the simulated array of the modeled quasi-tapered helical antenna elements.

As the radiation (or reception) patterns in Figs. 1(b) and 4(b) are analyzed; it's observed that the wavelength of operation changes the radiation pattern characteristics such as half-power beamwidth and side lobe levels. The maximum directivity of the model antennas becomes greater the shorter the wavelength of operation. This

observation coincides with the results of the model retinal receptor studies at microwave frequencies [51, 63]. Fig. 7 shows the normalized power patterns (directional patterns) of the modeled quasi-tapered helical antenna at different wavelengths of operation compared to the directional sensitivity of the human cones. The curve representative of the human cones is based on the formula of relative absorbed flux as $10 \cdot \log_{10} [0.25 \cdot (1 - \cos(0.95 \cdot \theta))^2]$ in decibels [51, 64]. The normalized power pattern with respect to $\theta$ is simply obtained by taking the square of the normalized amplitude of the computed electric field intensity of the modeled quasi-tapered helical antenna, regarding decibel calculations. Since there is no need to analyze side lobes for the comparison of the half-power beamwidths of the main lobes, the threshold level is kept at $-15$ dB, as it's also the case in [51]. In Fig. 7, the graphical results for the human cones and the modeled antenna at different wavelengths of operation do approximately coincide with each other.

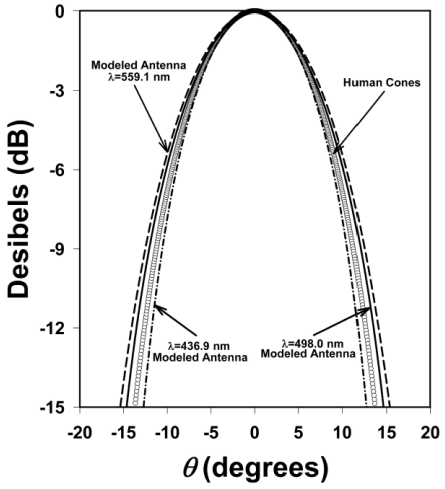


**Figure 7.** Comparison of the normalized power patterns ($E$-plane) of the modeled quasi-tapered helical antenna at different wavelengths of operation and the directional sensitivity of the human cones.

## 4. DISCUSSIONS AND CONCLUSIONS

The designed and simulated array of the modeled antennas is also suggested to be used in biomedical applications of the artificial retinal photoreceptors in medicine, for the future applications. Most current designs of retinal prostheses use photodiode-based technology to

capture light. Actually, the rod and cone cells could have been modeled by using receiving waveguide type antennas but an antenna-based approach will be a novel design in this field. Moreover, Sensiper [65] had analyzed helical antennas as a cylindrical waveguide model for determining the phase velocity term of propagating waves through the helical antennas. The modeled antennas can directly replace damaged photoreceptor cells. Positioning and fixing of the modeled antennas in the sub retinal space would be relatively easy; no external camera or external image processing is required; and eye movements can still be used to locate objects [66].

Although it seems to be an appropriate approach for retinal prostheses, fabrication of the modeled antennas is difficult. Dean et al. [67] used a micromachining technique called laser chemical vapor deposition (LCVD) to form fibers that can be grown into complex three-dimensional structures, such as helical antenna arrays operating in the frequency range from 100 GHz to over 2 THz. Billiet and Nguyen [68] have taken the patent about fabrication of arrays of ceramic embedded micro-electromagnetic devices as well as ceramic embedded helical micro-antennas designed for use in the high GHz and THz regions at a fraction of the present cost of manufacturing of such devices and with virtually no restriction to their miniaturization. There exist the specified fabrication techniques used for the helical antennas with up to 40 micron diameters at most [67] and antennas with fewer diameters will be harder to be fabricated, even impossible with current technologies. It can be noted that until higher nanoscale technologies are developed in the future, it almost won't be able to construct the modeled antennas with such small dimensions and geometries. It's obvious that the helical antenna models would be new among other current artificial photoreceptor technologies. However, until they are constructed and experimented, it's also impossible to make comparisons with the other current artificial photoreceptor technologies from advantages or disadvantages points of view. In addition, there has to be a transducer element combined within the antenna, such as metal-oxide-metal diode or microbolometer [69] to rectify the currents induced along the modeled antennas for helping the remaining living neuronal cells of the retina to process and conduct the electrical signals.

It can be easily emphasized that the light-sensitive cells are on the reverse direction for the incoming light. The pigment epithelium cells are responsible for phagocytosis and degradation of shed photoreceptor outer segments [70], and they are against the hazardous effects of light, particularly with the shorter wavelengths [71]. Beside these, it can be shown that the pigment epithelium cells are also effective in receiving

light waves. They reflect less than 1–2% of the incoming light waves in the reverse direction of the placement of the rod and cone cells [72]. There are functional and geometrical similarities between parabolic reflectors and the pigment epithelium cells. According to Fig. 1(b) and Fig. 4(b), the radiation intensity on the main lobe of the antennas is approximately equal to the average of the intensities of the light waves received by the minor lobes, regarding the 1–2% reflecting feature of the parabolic reflectors. The light wave intensities received by all sides of the antennas become approximately equal. Therefore, the photoreceptors or the simulated antennas are assumed to be operating in the region of both axial and normal modes. The analysis shows that the photoreceptors or the simulated antennas are also able to receive the reflected light waves from the pigment epithelium cells. Therefore, the pigment epithelium cells can be considered as parabolic reflectors.

In conclusion, new theoretical antenna models for the photoreceptors in the human retina have been proposed by using the analytic and modeling techniques in electromagnetic theory. The frequency responses of the simulated antennas have been approximately obtained the same as the spectral sensitivities of the photoreceptors. The study has analyzed that the spectral sensitivity of the photoreceptors is attributable to not just only visual pigments, but also should depend on the dimensions and geometrical shapes of the photoreceptors. The conical shapes of the cone cells should broaden the bandwidth of their spectral sensitivity; on the other hand the rod cells have narrower bandwidth, because of their cylindrical and uniform shapes. Beside, as analyzing the radiation (or reception) pattern of the modeled antenna array, it has been verified that the photoreceptor cells are arranged as an array to improve the spatial resolution. It's been also shown that the simulated power pattern characteristic of the modeled quasi-tapered helical antenna is very close to the directional sensitivity characteristic of the human cones. However, the suggested array of the modeled quasi-tapered helical antennas for the future biomedical applications of the artificial retinal photoreceptors is almost impossible to construct with current technologies.

## ACKNOWLEDGMENT

The authors thank Asst. Prof. Dr. Ahmet Kızılay for the useful discussions and help.

## REFERENCES


1. Sheppard, J. J., *Human Color Perception: A Critical Study of the Experimental Foundation*, American Elsevier, New York, 1968.
2. Tessier-Lavigne, M., "Phototransduction and information processing in the retina," *Principles of Neural Science*, 3 edition, E. R. Kandel, J. H. Schwartz, and T. M. Jessell (eds.), Prentice-Hall, Connecticut, 1991.
3. Wässle, H., "Colour vision — A patchwork of cones," *Nature*, Vol. 397, No. 6719, 473–475, 1999.
4. Feynman, R. P., R. B. Leighton, and M. Sands, *The Feynman Lectures on Physics*, Chapter 35, 36, Vol. I., Addison-Wesley, Boston, 1989.
5. Baylor, D., "Transduction in retinal photoreceptor cells," *Sensory Transduction: Society of General Physiologists — 45th Annual Symposium*, D. P. Corey and S. D. Roper, Vol. 47, Rockefeller University Press, New York, 1992.
6. Young, T., "The Bakerian lecture: On the theory of light and colours," *Philosophical Trans. Roy. Soc. Lond.*, Vol. 92, 12–48, 1802.
7. Rushton, W. A. H., "A cone pigment in the protanope," *J. Physiol.*, Vol. 168, No. 2, 345–359, 1963.
8. Marks, W. B., W. H. Dobelle, and E. F. Macnichol, Jr., "Visual pigments of single primate cones," *Science*, Vol. 143, No. 3611, 1181–1182, 1964.
9. Baylor, D. A., B. J. Nunn, and J. L. Schnapf, "The photocurrent, noise and spectral sensitivity of rods of the monkey Macaca fascicularis," *J. Physiol.*, Vol. 357, 575–607, Dec. 1984.
10. Nathans, J., D. Thomas, and D. S. Hogness, "Molecular genetics of human color vision: Genes encoding blue, green, and red pigments," *Science*, Vol. 232, No. 4747, 193–202, 1986.
11. Nathans, J., T. P. Piantanida, R. L. Eddy, T. P. Shows, and D. S. Hogness, "Molecular genetics of inherited variation in human color vision," *Science*, Vol. 232, No. 4747, 203–210, 1986.
12. Schnapf, J. L., T. W. Kraft, and D. A. Baylor, "Spectral sensitivity of human cone photoreceptors," *Nature*, Vol. 325, No. 6103, 439–441, 1987.
13. Eckmiller, M. S., "Cone outer segment morphogenesis: Taper change and distal invaginations," *J. Cell Biol.*, Vol. 105, No. 5, 2267–2277, 1987.
14. Palmer, S. E., *Vision Science: Photons to Phenomenology*, MIT

Press, Cambridge, 1999.

15. Miller, D., *The Wisdom of the Eye*, Academic Press, San Diego, 2000.
16. Roberts, N. W., "The optics of vertebrate photoreceptors: Anisotropy and form birefringence," *Vision Res.*, Vol. 46, No. 19, 3259–3266, 2006.
17. Warrant, E. J. and D.-E. Nilsson, "Absorption of white light in photoreceptors," *Vision Res.*, Vol. 38, No. 2, 195–207, 1998.
18. Kraus, J. D. and R. J. Marhefka, *Antennas for All Applications*, McGraw-Hill, New York, 2002.
19. Enoch, J. M., "Nature of the transmission of energy in the retinal receptors," *J. Opt. Soc. Am.*, Vol. 51, No. 10, 1122–1126, 1961.
20. Enoch, J. M., "Optical properties of the retinal receptors," *J. Opt. Soc. Am.*, Vol. 53, No. 1, 71–85, 1963.
21. Pask, C. and A. Stacey, "Optical properties of retinal photoreceptors and the Campbell effect," *Vision Res.*, Vol. 38, No. 7, 953–961, 1998.
22. Hajiaboli, A. and M. Popović, "FDTD analysis of light propagation in the human photoreceptor cells," *IEEE Trans. Magnetics*, Vol. 44, No. 6, 1430–1433, 2008.
23. Gouras, P., "Color vision," *Principles of Neural Science*, 3 edition, E. R. Kandel, J. H. Schwartz, and T. M. Jessell (eds.), Prentice-Hall, Connecticut, 1991.
24. Wald, G., "Blue-blindness in the normal fovea," *J. Opt. Soc. Am.*, Vol. 57, No. 11, 1289–1301, 1967.
25. Logvinenko, A. D., "On derivation of spectral sensitivities of the human cones from trichromatic colour matching functions," *Vision Res.*, Vol. 38, No. 21, 3207–3211, 1998.
26. Lee, K.-F., P.-F. Wong, and K.-F. Larm, "Theory of the frequency responses of uniform and quasi-taper helical antennas," *IEEE Trans. Antennas Propag.*, Vol. 30, No. 5, 1017–1021, 1982.
27. Grand, Y. L., *Light, Colour and Vision*, Chapman & Hall, London, 1968.
28. Kraus, J. D. and D. A. Fleisch, *Electromagnetics with Applications*, McGraw-Hill, Singapore, 1999.
29. Gabriel, C., S. Gabriel, and G. Corthout, "The dielectric properties of biological tissues: III. parametric models for the dielectric spectrum of tissues," *Phys. Med. Biol.*, Vol. 41, No. 11, 2271–2293, 1996.
30. Canbay, C., *Anten ve Propagasyon I*, Yeditepe University Press, İstanbul, 1997.

31. Challa, R. K., D. Kajfez, J. R. Gladden, A. Z. Elsherbeni, and V. Demir, "Permittivity measurement with a non-standard waveguide by using TRL calibration and fractional linear data fitting," *Progress In Electromagnetics Research B*, Vol. 2, 1–13, 2008.
32. Kumar, A., S. Sharma, and G. Singh, "Measurement of dielectric constant and loss factor of the dielectric material at microwave frequencies," *Progress In Electromagnetics Research*, PIER 69, 47–54, 2007.
33. King, H. E. and J. L. Wong, "Characteristics of 1 to 8 wavelength uniform helical antennas," *IEEE Trans. Antennas Propag.*, Vol. 28, No. 2, 291–296, 1980.
34. Emerson, D. T., "The gain of an axial-mode helix antenna," *The ARRL Antenna Compendium*, Vol. 4, 64–68, 1995.
35. Sinclair, G., "Theory of models of electromagnetic systems," *Proc. IRE*, Vol. 36, No. 11, 1364–1370, 1948.
36. Brindley, G. S., *Physiology of the Retina and Visual Pathway*, Camelot Press, London, 1970.
37. Holcman, D. and J. I. Korenbrot, "Longitudinal diffusion in retinal rod and cone outer segment cytoplasm: The consequence of cell structure," *Biophysical Journal*, Vol. 86, No. 4, 2566–2582, 2004.
38. Wong, J. L. and H. E. King, "Broadband quasi-taper helical antennas," *IEEE Trans. Antennas Propag.*, Vol. 27, No. 1, 72–78, 1979.
39. Nakano, H., N. Ikeda, and J. Yamauchi, "Quadrifilar conical helical antenna with travelling-wave current distribution," *IEE Proc. - Microwaves, Antennas and Propag.*, Vol. 144, No. 1, 53–55, 1997.
40. Dobbins, J. A. and R. L. Rogers, "Folded conical helix antenna," *IEEE Trans. Antennas Propag.*, Vol. 49, No. 12, 1777–1781, 2001.
41. Seluk, A. and B. Saka, "A general method for the analysis of curved wire antennas," *Journal of Electromagnetic Waves and Applications*, Vol. 21, No. 2, 175–188, 2007.
42. Zhang, Y., J. Wang, Z. Zhao, and J. Yang, "The analysis of LPDA using MoM and transmission matrix," *Journal of Electromagnetic Waves and Applications*, Vol. 21, No. 12, 1621–1633, 2007.
43. Shafieha, J. H., J. Noorinia, and Ch. Ghobadi, "Probing the feed line parameters in Vivaldi Notch Antennas," *Progress In Electromagnetics Research B*, Vol. 1, 237–252, 2008.
44. Rajabi, M., M. Mohammadirad, and N. Komjani, "Simulation of ultra wideband microstrip antenna using EPML-TLM," *Progress*

*In Electromagnetics Research B*, Vol. 2, 115–124, 2008.

45. Yu, Y. K. and J. Li, "Analysis of electrically small size conical antennas," *Progress In Electromagnetics Research Letters*, Vol. 1, 85–92, 2008.
46. Chen, Y.-L., C.-L. Ruan, and L. Peng, "A novel ultra-wideband bow-tie slot antenna in wireless communication systems," *Progress In Electromagnetics Research Letters*, Vol. 1, 101–108, 2008.
47. Gao, G.-P., X.-X. Yang, J.-S. Zhang, and J.-X. Xiao, "A printed volcano smoke antenna for UWB and WLAN communications," *Progress In Electromagnetics Research Letters*, Vol. 4, 55–61, 2008.
48. Kraft, U. R. and G. Mnich, "Main-beam polarization properties of modified helical antennas," *IEEE Trans. Antennas Propag.*, Vol. 38, No. 5, 589–597, 1990.
49. Blieske, U., T. Doege, P. Gayout, M. Neander, D. Neumann and A. Prat, "Light-trapping in solar modules using extra-white textured glass," *Proc. 3rd World Conference on Photovoltaic Energy Conversion*, Vol. 1, 188–191, Osaka, May 2003.
50. Snyder, A. W. and P. A. V. Hall, "Unification of electromagnetic effects in human retinal receptors with three pigment colour vision," *Nature*, Vol. 223, No. 5205, 526–528, 1969.
51. Enoch, J. M. and G. A. Fry, "Characteristics of a model retinal receptor studied at microwave frequencies," *J. Opt. Soc. Am.*, Vol. 48, No. 12, 899–911, 1958.
52. Oughstun, K. E., "Pulse propagation in a linear, causally dispersive medium," *Proc. IEEE*, Vol. 79, No. 10, 1379–1390, 1991.
53. Hillion, P., "Electromagnetic pulses in dispersive media," *Progress In Electromagnetics Research*, PIER 18, 245–260, 1998.
54. Margetis, D., "Pulse propagation in sea water: The modulated pulse," *Progress In Electromagnetics Research*, PIER 26, 89–110, 2000.
55. Koester, J., "Voltage-gated ion channels and the generation of the action potential," *Principles of Neural Science*, 3 edition, E. R. Kandel, J. H. Schwartz, and T. M. Jessell (eds.), Prentice-Hall, Connecticut, 1991.
56. Roorda, A., A. B. Metha, P. Lennie, and D. R. Williams, "Packing arrangement of the three cone classes in primate retina," *Vision Res.*, Vol. 41, No. 10, 1291–1306, 2001.
57. Roorda, A. and D. R. Williams, "The arrangement of the three cone classes in the living human eye," *Nature*, Vol. 397, No. 6719,

520–522, 1999.

58. Lennie, P., "Color vision: Putting it together," *Curr. Biol.*, Vol. 10, No. 16, 589–591, 2000.
59. Balanis, C. A., *Antenna Theory, Analysis and Design*, John Wiley & Sons, New York, 1997.
60. Mariani, A. P., "The neuronal organization of the outer plexiform layer of the primate retina," *Int. Rev. Cytol.*, Vol. 86, 285–320, 1984.
61. Ahnelt, P. K., H. Kolb, and R. Pflug, "Identification of a subtype of cone photoreceptor, likely to be blue sensitive, in the human retina," *J. Comp. Neurol.*, Vol. 255, No. 1, 18–34, 1987.
62. Laughlin, S. B., "Retinal function: Coupling cones clarifies vision," *Curr. Biol.*, Vol. 12, No. 24, 833–834, 2002.
63. Enoch, J. M., "Response of a model retinal receptor as a function of wavelength," *J. Opt. Soc. Am.*, Vol. 50, No. 4, 315–320, 1960.
64. Enoch, J. M., "Summated response of the retina to light entering different parts of the pupil," *J. Opt. Soc. Am.*, Vol. 48, No. 6, 392–405, 1958.
65. Sensiper, S., "Electromagnetic wave propagation on helical conductors," *Proc. IRE*, Vol. 43, No. 2, 149–161, 1955.
66. Zrenner, E., "Will retinal implants restore vision?" *Science*, Vol. 295, No. 5557, 1022–1025, 2002.
67. Dean, Jr., R. N., P. C. Nordine, and C. G. Christodoulou, "3-D helical THz antennas," *Microw. Opt. Tech. Lett.*, Vol. 24, No. 2, 106–111, 2000.
68. Billiet, R. L. and H. T. Nguyen, "Ceramic-embedded micro-electromagnetic device and method of fabrication thereof," U.S. Patent, Patent No: 6 693 601, 2004.
69. Alda, J., J. M. Rico-Garcia, J. M. Lopez-Alonzo, and G. Boreman, "Optical antennas for nano-photonic applications," *Nanotechnology*, Vol. 16, No. 5, 230–234, 2005.
70. Liang, F.-Q., L. Green, C. Wang, R. Alssadi, and B. F. Godley, "Melatonin protects human retinal pigment epithelial (RPE) cells against oxidative stress," *Exp. Eye Res.*, Vol. 78, No. 6, 1069–1075, 2004.
71. Gurney, P. W. V., "Is our 'inverted' retina really 'bad design'?" *Technical Journal–in-depth Journal of Creation*, Vol. 13, No. 1, 37–44, 1999.
72. Preece, S. J. and E. Claridge, "Monte Carlo modelling of the spectral reflectance of the human eye," *Phys. Med. Biol.*, Vol. 47, No. 16, 2863–2877, 2002.